ECCM-2001
European Conference on
Computational Mechanics

June 26-29, 2001
Cracow, Poland

Comparison of two classes of integration algorithms in creep analysis

Pekka Marjamäki, Jorma Kivilahti

Laboratory of Electronics Production Technology
Helsinki University of Technlogy, Espoo, Finland
e–mail: pekka.marjamaki@hut.fi, jorma.kivilahti@hut.fi

Reijo Kouhia

Laboratory of Structural Mechanics
Helsinki University of Technology, Espoo, Finland
e–mail: reijo.kouhia@hut.fi

Key words: creep, viscoplasticity, time integration algorithms, explicit, implicit

Abstract. *Applicability of both explicit and implicit integration algorithms for creep analysis of solder joints is evaluated. Two recently published methods has been compared for considering both accuracy and computational labor.*

1 Introduction

Increased packaging density of electronic components on printed wiring boards (PWBs) has raised mechanical reliability concerns. The thermomechanical problems are mainly induced by the mismatch of the thermal expansion coefficients between the individual components and the board. Since empirical methods are time consuming computational modelling is increasingly used to assess the response and reliability of electronic devices.

Computational modelling of solder materials is difficult. In general, solder is a viscoplastic material in which the material parameters depend upon the microstructure. Processing influences the initial microstructure which then changes during the thermomechanical loading process induced by the electrical functioning of the product.

The trend of using more and more complex material models makes their integration a delicate problem. Many different algorithms exist, however, the fully implicit methods has today become the 'canonical' method of choice. On the other hand, if accuracy and easyness of adapting new material models into the integration routine is considered, the backward Euler method seems not to be so ideal. Recently Wallin and Ristinmaa [1] have proposed a rather general setting for integrating path-dependent material responces. Their paper was focused towards rate-independent problems, in this study it has been used for rate-dependent creep type analysis. Schreyer [2] has proposed an implicit integration based on generalized trapezoidal rule. The essential feature of his method is to use the steady state solution instead of the solution at the end of the previous step as a initial value for the Newton's iteration.

In this study the explicit methodology of Wallin and Ristinmaa is compared to the implicit approach of Schreyer. Both accuracy and total computation labor is considered in some example cases on thermal stress analysis of solder joints using the constitutive models described in the subsequent section.

2 Material models

Quite a few viscoplastic material models have been developed for solder alloys. A rather popular constitutive model in solder joint reliability computations has been developed by Anand and Brown [3], [4]

$$\boldsymbol{\epsilon}^{\text{in}} = \tfrac{3}{2}\gamma \boldsymbol{n} = \tfrac{3}{2} f \exp\left(\frac{-Q}{R\theta}\right) \sinh^m\left(\frac{\tau}{Y}\right) \boldsymbol{n}, \tag{1}$$

where f, m and Q are material parameters, R is the gas constant and θ the absolute temperature. The scalar τ is the equivalent stress. This model can account for strain rate and temperature sensitivity and the dynamic recovery processes. It uses single internal parameter, Y, which represents the averaged isotropic resistance to macroscopic plastic flow offered by the underlying isotropic strenghtening mechanisms such as solid solution strenghtening and grain size effects.

The evolution equation for the "flow stress" used in ref. [3] is

$$\dot{Y} = H_1(|1 - Y/\tilde{Y}|)^{H_2} \text{sign}(1 - Y/\tilde{Y})\gamma,$$

where $\tilde{Y}$ is the saturation value of Y and is a function of the deformation rate

$$\tilde{Y} = H_3 \left[\frac{\gamma}{f} \exp\left(\frac{-Q}{R\theta} \right) \right]^n .$$

To make the grain-coarsening more explicit an internal state model taking into account hardening, recovery and grain coarsening has been developed in refs. [5], [6]. In this model the inelastic strain rate, $\dot{\boldsymbol{\epsilon}}^{\text{in}}$, is given by

$$\dot{\boldsymbol{\epsilon}}^{\text{in}} = \tfrac{3}{2} f \exp\left(\frac{-Q}{R\theta} \right) \left(\frac{\lambda_0}{\lambda} \right)^p \sinh^m \left(\frac{\tau}{\sigma_y} \right) \boldsymbol{n} \tag{2}$$

where f, p, m and Q are material parameters, R is the gas constant, θ the absolute temperature, λ, λ_0 are the current and initial grain sizes (average diameters) and σ_y is the "flow stress". The scalar τ is the reduced equivalent stress

$$\tau = \sqrt{\tfrac{3}{2} \boldsymbol{\tau} : \boldsymbol{\tau}} = \sqrt{\tfrac{3}{2} \left(\boldsymbol{s} - \tfrac{2}{3} \boldsymbol{B} \right) : \left(\boldsymbol{s} - \tfrac{2}{3} \boldsymbol{B} \right)},$$

where $\boldsymbol{s}$ is the stress deviator and $\boldsymbol{B}$ is the back stress accounting for the kinematic hardening and the direction of the flow, $\boldsymbol{n}$, is defined as: $\boldsymbol{n} = (\boldsymbol{s} - \frac{2}{3}\boldsymbol{B})/\tau$.

In refs. [5], [6] the Hall-Petch type dependency of the flow stress on the grain size is used

$$\sigma_y = Y + k(\lambda_0/\lambda)^\beta, \tag{3}$$

where the material parameters Y, k and β depend on temperature. The grain size growth rate $\dot{\lambda}$ depends on the current grain size and, according to Clark and Alden [7], is proportional to the excess vacancy concentration c_v^x. The evolution equations for the grain size and excess vacancy concentration are:

$$\dot{\lambda} = A \frac{c_v^x + c_v^0}{\lambda}, \qquad \dot{c}_v^x = B\gamma - C c_v^x, \tag{4}$$

where A, B and C are material parameters, and c_v^0 is the equilibrium vacancy concentrations.

Rather complex hardening rules, adapted from the constitutive model of Miller [8], are used in refs. [2], [5], [6]:

$$\dot{Y} = H_1\gamma - (H_2\gamma + H_3)(Y - Y_0)^2, \qquad \dot{\boldsymbol{B}} = K_1 \dot{\boldsymbol{\epsilon}}^{\text{in}} - (K_2\gamma + K_3) \left(\sqrt{\tfrac{2}{3} \boldsymbol{B} : \boldsymbol{B}} \right) \boldsymbol{B},$$

where $H_1, ..., H_3, K_1, ..., K_3$ and Y_0 are material parameters. The material parameter K_1 provides a measure how closely the rate of the backstress tracks the inelastic strain rate while the parameters K_2 and K_3 are associated with the dynamic and static recovery, respectively, of the backstress.

3 Integration algorithms

The coverning set of evolution equations for the model (1) is

$$\begin{aligned} \dot{\boldsymbol{s}} =& 2G(\dot{\boldsymbol{e}} - \dot{\boldsymbol{\epsilon}}^{\text{in}}), \\ \dot{Y} =& H_1(|1 - Y/\tilde{Y}|)^{H_2}\text{sign}(1 - Y/\tilde{Y})\gamma, \end{aligned} \tag{5}$$

where $\dot{\boldsymbol{e}}$ is the deviatoric strain rate and G the shear modulus. Ignoring the effect of grain growth the system for the model (2) is the following:

$$\begin{aligned} \dot{\boldsymbol{s}} &= 2G(\dot{\boldsymbol{e}} - \dot{\boldsymbol{\epsilon}}^{\text{in}}), \\ \dot{\boldsymbol{B}} &= K_1\dot{\boldsymbol{\epsilon}}^{\text{in}} - (K_2\gamma + K_3)\left(\sqrt{\tfrac{2}{3}\boldsymbol{B} : \boldsymbol{B}}\right)\boldsymbol{B}, \\ \dot{Y} &= H_1\gamma - (H_2\gamma + H_3)(Y - Y_0)^2. \end{aligned} \tag{6}$$

3.1 Explicit methods

In solving systems like (5) and (6) explicit methods are attractive due to their simplicity. In integrating non-linear material models with explicit methods, subincrementing is commonly used within each time step Δt, see refs. [9], [10]. The simplest time integrator is the forward Euler scheme

$$\boldsymbol{y}_{n+1} = \boldsymbol{y}_n + \sum_{i=1}^{k} \delta t_i \dot{\boldsymbol{y}}_{n,i}, \qquad \Delta t = t_{n+1} - t_n = \sum_{i=1}^{k} \delta t_i,$$

where $\boldsymbol{y} = (\boldsymbol{s}\ Y)^T$ or $\boldsymbol{y} = (\boldsymbol{s}\ \boldsymbol{B}\ Y)^T$ for model (1) and (2), respectively. Addition of grain growth and other state variables into the system is simple. Unfortunately the forward Euler method is only first order accurate.

More advanced schemes like the Runge-Kutta methods have also been considered, see e.g. refs. [1], [11], [12]. The general form of the Runge-Kutta method can be written as

$$\begin{aligned} \boldsymbol{y}_{n+1} &= \boldsymbol{y}_n + \sum_{i=1}^{s} b_i \boldsymbol{k}_i, \\ \boldsymbol{k}_1 &= \Delta t \dot{\boldsymbol{y}}_n, \\ \boldsymbol{k}_i &= \Delta t \dot{\boldsymbol{y}}(t_n + c_i\Delta t, \boldsymbol{y}_n + \sum_{j=1}^{i-1} a_{ij}\boldsymbol{k}_j), \end{aligned}$$

where $a_{ij},\ b_i$ and c_i are coefficients. One algorithm which have been successfully used in elasto-plastic computations [12] is the Runge-Kutta-Dormand-Prince (DOPRI) method, introduced by Dormand and Prince [13]. It uses seven stages and its local truncation error is of fourth order.

The DOPRI algorithm belongs to the family of embedded Runge-Kutta methods, which means that higher order estimate, $\bar{\boldsymbol{y}}_{n+1} = \boldsymbol{y}_n + \sum_{i=1}^{s} \bar{b}_i \boldsymbol{k}_i$, for the solution can be obtained without any extra function evaluations. An estimate of the error is obtained by computing the difference $\boldsymbol{y}_{n+1} - \bar{\boldsymbol{y}}_{n+1}$ which can be used for step length adaptation. The coefficients a_{ij}, b_i and c_i of the DOPRI method are shown in Table 1.

			a_{ij}				c_i	b_i
i	$j=1$	2	3	4	5	6		
1							0	$\frac{5179}{57600}$
2	$\frac{1}{5}$						$\frac{1}{5}$	0
3	$\frac{3}{40}$	$\frac{9}{40}$					$\frac{3}{40}$	$\frac{7571}{16695}$
4	$\frac{44}{45}$	$-\frac{56}{15}$	$\frac{32}{9}$				$\frac{4}{5}$	$\frac{393}{640}$
5	$\frac{19372}{6561}$	$-\frac{25360}{2187}$	$\frac{64448}{6561}$	$-\frac{212}{729}$			$\frac{8}{9}$	$-\frac{92097}{339200}$
6	$\frac{9017}{3168}$	$-\frac{355}{33}$	$\frac{46732}{5247}$	$\frac{49}{176}$	$-\frac{5103}{18656}$		1	$\frac{187}{2100}$
7	$\frac{35}{384}$	0	$\frac{500}{1113}$	$\frac{125}{192}$	$-\frac{2187}{6784}$	$\frac{11}{84}$	1	$\frac{1}{40}$

Table 1: Coefficients for the DOPRI method.

3.2 Implicit method

The main disadvantage of explicit methods is that they are only conditionally stable, and the critical time step may be several orders of magnitude smaller that the desired time step. Schreyer [2] used the generalized trapezoidal rule to solve the evolution equations, like (5) or (6). He also used the steady state solution as an initial guess for the Newton-Raphson iteration.

In the following, the Schreyer's algorithm is described only for the model (2). Modification of the expressions to the model (1) is trivial. Denoting $\boldsymbol{\tau} = \boldsymbol{s} - \frac{2}{3}\boldsymbol{B}$ and applying the generalized trapezoidal rule to the evolution equations (6) results in

$$\begin{aligned}
\boldsymbol{\tau}_{n+1} &= \boldsymbol{\tau}_n + \Delta t\big(\alpha\dot{\boldsymbol{\tau}}_{n+1} + (1-\alpha)\dot{\boldsymbol{\tau}}_n\big),\\
\boldsymbol{B}_{n+1} &= \boldsymbol{B}_n + \Delta t\big(\alpha\dot{\boldsymbol{B}}_{n+1} + (1-\alpha)\dot{\boldsymbol{B}}_n\big),\\
Y_{n+1} &= Y_n + \Delta t\big(\alpha\dot{Y}_{n+1} + (1-\alpha)\dot{Y}_n\big).
\end{aligned}$$

Following the formulation in ref. [2], solution of this nonlinear system can be performed involving only the scalar "invariants" τ and B and the flow stress Y. The resulting nonlinear algebraic system is

$$\begin{aligned}
F_1 =& \tau_{n+1}D - \sqrt{1.5 f_1} = 0,\\
F_2 =& B_{n+1}D - \sqrt{2/3\ f_2} = 0,\\
F_3 =& Y_{n+1} - Y_n - \Delta t\alpha\left[K_1\gamma_{n+1} + (K_2\gamma_{n+1} + K_3)(Y_{n+1} - Y_0)^2\right]\\
&- \Delta t(1-\alpha)\left[K_1\gamma_n + (K_2\gamma_n + K_3)(Y_n - Y_0)^2\right] = 0,
\end{aligned} \tag{7}$$

where

$$\begin{aligned}
\tau &= \sqrt{\tfrac{3}{2}\left(\boldsymbol{s} - \tfrac{2}{3}\boldsymbol{B}\right) : \left(\boldsymbol{s} - \tfrac{2}{3}\boldsymbol{B}\right)},\\
B &= \sqrt{\tfrac{2}{3}\boldsymbol{B} : \boldsymbol{B}},\\
D &= 1 + \Delta t\alpha(A_{11,n+1} + A_{22,n+1}) + (\Delta t)^2\alpha^2(A_{11,n+1}A_{22,n+1} - A_{12,n+1}A_{21,n+1}),
\end{aligned}$$

$$
\begin{aligned}
f_1 &= (1+\Delta t\alpha A_{22,n+1})^2 R_{11} - 2(1+\Delta t\alpha A_{22,n+1})\Delta t\alpha A_{12,n+1} R_{12} \\
&\quad +(\Delta t)^2\alpha^2 \left(A_{11,n+1}\right)^2 R_{22}, \\
f_2 &= (\Delta t)^2\alpha^2 \left(A_{11,n+1}\right)^2 R_{11} - 2(1+\Delta t\alpha A_{11,n+1})\Delta t\alpha A_{21,n+1} R_{12} \\
&\quad +(1+\Delta t\alpha A_{11,n+1})^2 R_{22}, \\
R_{ij} &= \boldsymbol{R}_i : \boldsymbol{R}_j, \\
\boldsymbol{R}_1 &= [1-\Delta t(1-\alpha)A_{11,n}]\,\boldsymbol{\tau}_n - \Delta t(1-\alpha)A_{12,n}\boldsymbol{B}_n + \Delta t\alpha\,\dot{\boldsymbol{s}}^{\mathrm{el}}_{n+1} + \Delta t(1-\alpha)\dot{\boldsymbol{s}}^{\mathrm{el}}_n, \\
\boldsymbol{R}_2 &= -\Delta t(1-\alpha)A_{21,n}\boldsymbol{\tau}_n + [1-\Delta t(1-\alpha)A_{22,n}]\,\boldsymbol{B}_n, \\
\dot{\boldsymbol{s}}^{\mathrm{el}} &= 2G\dot{\boldsymbol{e}}, \\
A_{11} &= (3G+K_1)\frac{\gamma}{\tau}, \qquad A_{12} = -\tfrac{2}{3}(K_2\gamma + K_3)B, \\
A_{21} &= -K_1\frac{3\gamma}{2\tau}, \qquad A_{22} = (K_2\gamma + K_3)B.
\end{aligned}
$$

The formulas for A_{ij}, F_1 and F_2 differ slightly from those presented in ref. [2] due to the difference in defining the direction of the inelastic deformation $\boldsymbol{n}$.

As already mentioned, grain growth is assumed to be slow, thus it is not included in the system (7). The grain size and vacancy concentration are updated according to equations (4) after the Newton iteration of the system (7) is converged.

As argued in ref. [2], the use of the steady state-solution for the initial guess appears to be within the radius of convergence of the Newton-Raphson iteration. The steady-state solution is obtained under the assumptions that $\dot{\boldsymbol{\tau}}$, $\dot{\boldsymbol{B}}$ and $\dot{Y}$ are zero and the elastic deviatoric "trial" stress $\dot{\boldsymbol{s}}^{\mathrm{el}}$ is constant. This is obtained if

$$
\begin{aligned}
\dot{\boldsymbol{e}} &= \dot{\boldsymbol{\epsilon}}^{\mathrm{in}}, \\
\gamma_{ss} &= \sqrt{\dot{\boldsymbol{e}} : \dot{\boldsymbol{e}}}, \\
Y_{ss} &= \sqrt{H_1\gamma_{ss}/(H_2\gamma_{ss}+H_3)} + Y_0,
\end{aligned}
$$

and τ_{ss} can be solved from equation (1) or (2). The steady-state solution for the invariant of the initial backstress is

$$
B^2_{ss} = \frac{K_1\gamma_{ss}}{K_2\gamma_{ss}+K_3}.
$$

4 Example

Performance of the described schemes in a simple uniaxial stretching test of a cube ($1\times1\times1$ mm^3) is compared. The material data is taken from ref. [6], which represents mechanical properties of the binary near eutectic Sn40Pb solder, see Table 2. However, the grain diameter dependency from the flow stress has been neglected as well as the kinematic and isotropic hardening effects. Isothermal conditions are assumed ($\theta = 293$ K). The cube is modelled using a single trilinear standard isoparametric element.

The loading is applied by prescribing the axial displacements at the loaded face. Different strain rates are used in the computations.

E	=	33 GPa	Q	=	12 kcal/mol
ν	=	0.3	R	=	$2{\cdot}10^{-3}$ kcal/mol·K
σ_0	=	20 MPa	f	=	10^5 s^{-1}
m	=	3.5	c_v^0	=	10^{-9}
p	=	2	A	=	$3.74{\cdot}10^4$ (μm)^{2}s^{-1}
λ_0	=	30 μm	B	=	$4.1{\cdot}10^{-3}$ s^{-1}
k	=	0	C	=	$1.67{\cdot}10^{-2}$ s^{-1}

Table 2: Material parameters of the binary near eutectic Sn40Pb solder.

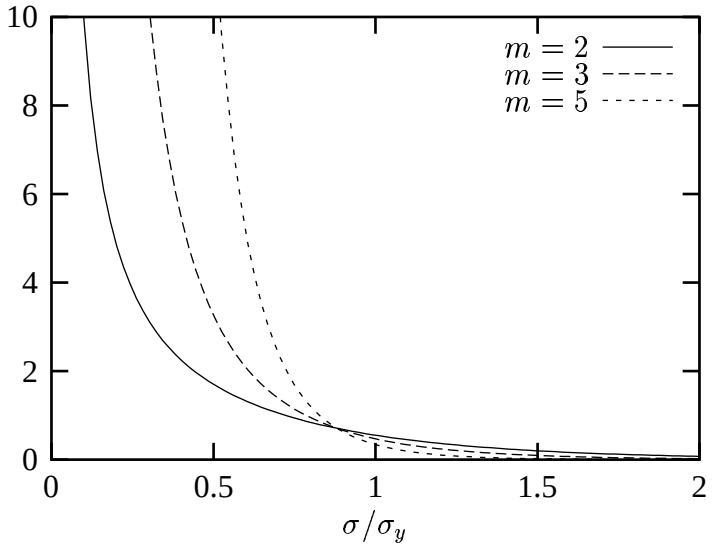

Figure 1: Function $\mathcal{F}(\sigma/\sigma_y)$.

In the uniaxial case, the material behaviour is described by scalar equation

$$\dot{\sigma} + E\tilde{f}\sinh^m\left(\frac{\sigma}{\sigma_y}\right) = E\dot{\epsilon}, \tag{8}$$

where E is the Young's modulus and $\tilde{f} = f\exp(-Q/R\theta)(\lambda_0/\lambda)^p$. The critical time step for the explicit Euler scheme of the linearized form of the equation (8) is

$$\Delta t_{\mathrm{cr}} = \frac{2}{m\tilde{f}}\left(\frac{\sigma_y}{E}\right)\frac{1}{\sinh^{m-1}(\sigma/\sigma_y)\cosh(\sigma/\sigma_y)} = \frac{2}{m\tilde{f}}\left(\frac{\sigma_y}{E}\right)\mathcal{F}(\sigma/\sigma_y),$$

and the behaviour of the function $\mathcal{F}$ is shown in fig. 1. For the material parameters shown in Table 2, the value of $2\sigma_y/(m\tilde{f}E) \approx 2.7$ s. The critical times step for explicit schemes can thus vary several orders of magnitude, depending on the state, as also pointed out in ref. [2].

Some results from computations with strain rates of 10^{-3}, 10^{-4} and 10^{-5} are shown in figs. 2 – 4. The reference solution is obtained by the DOPRI method with 1000 equal size time steps.

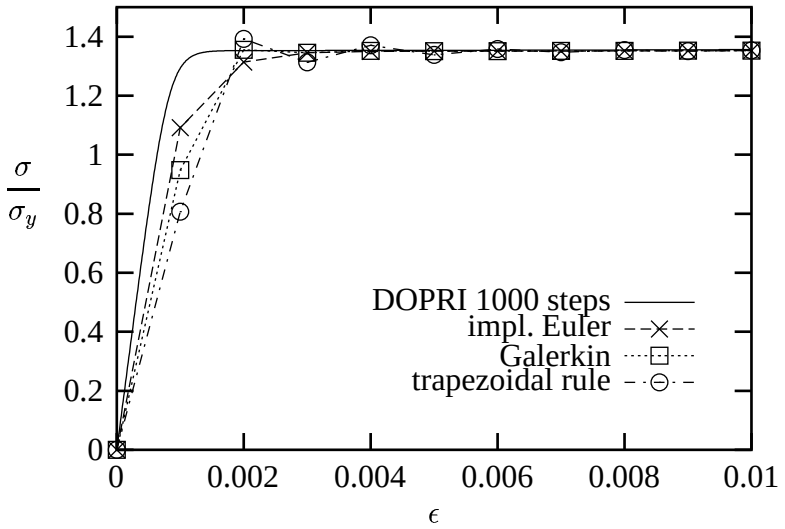

Figure 2: Computed stress-strain relationship of the Sn40Pb solder with strain rate $\dot{\epsilon} = 10^{-3}$.

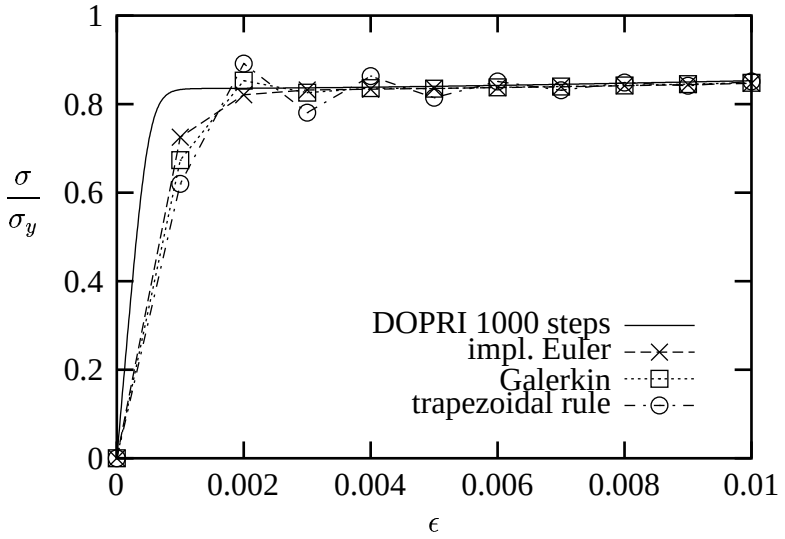

Figure 3: Computed stress-strain relationship of the Sn40Pb solder with strain rate $\dot{\epsilon} = 10^{-4}$.

For the implicit schemes (backward Euler $\alpha = 1$, Galerkin $\alpha = \frac{2}{3}$ and trapezoidal rule $\alpha = \frac{1}{2}$), ten equal time steps are used in all cases. Therefore the time steps used for the implicit schemes are 1 s, 10s and 100 s in computations with strain rates 10^{-3}, 10^{-4} and 10^{-5}, respectively. It is clearly seen, that the trapezoidal rule gives oscillating solutions, especially in the slow strain rate case ($\dot{\epsilon} = 10^{-5}$) when the time step is 100 s, which is much larger than the oscillating limit, i.e. the critical time step of the explicit Euler scheme.

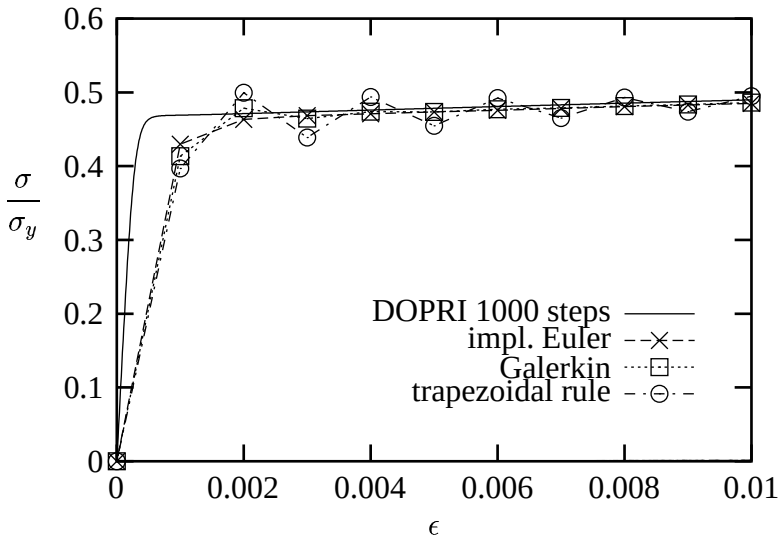

Figure 4: Computed stress-strain relationship of the Sn40Pb solder with strain rate $\dot{\epsilon} = 10^{-5}$.

	$\dot{\epsilon}$		
	10^{-3}	10^{-4}	10^{-5}
Δt	1 s	10 s	100 s
implicit Euler	-0.25	-0.7	-1.0
Galerkin	-0.24	-0.6	-0.8
trapezoidal rule	-0.16	-0.2	$+1.0$

Table 3: Difference in per cent on the solution with respect to the DOPRI method at 1% strain.

Using the solutions obtained by the DOPRI method as a reference, the difference to the values from implicit computations are shown in Table 3 which give some estimate on the solution error at the end of the computation. Due to the asymptotic quadratic accuracy, the trapezoidal rule is clearly the most accurate as compared to the Galerkin and the backward Euler schemes. However, the Galerkin method appear to be slightly better than the other schemes when larger time steps are used. As it is well know, the accuracy of the trapezoidal rule deteriorates when the time steps gets larger, since the amplification factor aproaches to -1 as $\Delta t \longrightarrow \infty$.

For softening stress-strain relationship, the trapezoidal rule is only conditionally stable, therefore the midpoint version is preferable. This, as well as other computational issues will be addressed in a subsequent paper.

5 Concluding remarks

The model (2) can predict the grain coarsening effect. However, there is evidence that the solder alloys can behave in a very ductile manner, even exhibiting superplastic behaviour. Shear-band formation have been observed in experiments, see ref. [14], figure 5 page 215. For superplastic behaviour to occur recrystallisation has necessarily to happen. However, the model (2) cannot simulate recrystallisation. In addition, the use of the Hall-Petch equation (3) is questionable; it is mainly developed for steels and it predicts larger flow stresses when the grain size is decreased, which is in contradiction to behaviour observed in superplastic materials.

The ongoing research will focus on the development of a microstructurally based constitutive model which should be able to predict the grain growth as well as the recrystallisation processes. In addition, damage evolutiong of solder materials should also be accounted for in order to obtain realistic life-time predictions of electronic products.

Explicit time integrators provides simple and attractive schemes for testing new time-dependent material models. However, due to the conditional stability of explicit methods, they are not feasible in real life production computations. Usually, either the implicit backward Euler or the trapezoidal rules are used. Nevertheless, these methods also suffer from serious deficiences; the implicit Euler is only first order accurate and the trapezoidal rule, although second order accurate, produces severe oscillations when the time step is larger than the critical time step of the explicit Euler scheme. In a further study the use of higher order implicit single step method will be examined.

References

[1] M. Wallin and M. Ristinmaa. Accurate stress updating algorithm based on constant strain rate assumption. manuscript.

[2] H.L. Schreyer. Unconditionally stable time integration of creep constitutive equations. Eccomas 2000, Barcelona 11-14 September 2000, CD-ROM Proceedings.

[3] L. Anand and S. Brown. Constitutive equations for large deformations of metals at high temperatures. In J. Chandra and R.P. Srivastav, editors, *Constitutive Models of Deformation*, pages 1–26, (1987).

[4] S.B. Brown, K.H. Kim, and L. Anand. An internal variable constitutive model for hot working of metals. *International Journal of Plasticity*, 5:91–130, (1989).

[5] D.R. Frear, S.N. Burchett, M.K. Neilsen, and J.J. Stephens. Microstructurally based finite element simulation of solder joint behaviour. *Soldering & Surface Mount Technology*, 1(25):39–42, (1997).

[6] S.N. Burchett, M.K. Neilsen, D.R. Frear, and J.J. Stephens. Computational continuum modelling of solder interconnects. In R.K. Mahidhara et al., editor, *Design and Reliability of Solders and Solder Interconnects*, pages 171–178, The Minerals, Metals & Materials Society, (1997).

[7] M.A. Clark and T.H. Alden. Deformation enhanged grain growth in a superplastic Sn-1% Bi alloy. *Acta Metallurgica*, 21:1195–1206, (1973).

[8] A. Miller. An inelastic constitutive model for monotonic, cyclic and creep deformations: Part I – equations development and analytical procedures. *Journal of Engineering Materials Technology*, 98:97–105, (1976).

[9] O.C. Zienkiewicz and R.L. Taylor. *The Finite Element Method*, Volume 2, Fourth edition, McGraw-Hill, (1991).

[10] K.-J. Bathe. *Finite Element Procedures*. Prentice Hall, (1996).

[11] S.W. Sloan. Substepping schemes for the numerical integration of elastoplastic stress-strain relations. *International Journal for Numerical Methods in Engineering*, 24:893–911, (1987).

[12] S.W. Sloan and J.R. Booker. Integration of Tresca and Mohr-Coulomb constitutive relations in plain strain elasticity. *International Journal for Numerical Methods in Engineering*, 33:163–196, (1992).

[13] J.R. Dormand and P.J. Prince. A family of embedded Runge-Kutta formulae. *Journal of Computational and Applied Mathematics*, 6:19–26, (1980).

[14] G. Grossmann and L. Weber. Metallurgical considerations for accelerated testing of soft solder joints. *IEEE Transactions on Components, Packaging, and Manufacturing Technology - Part C*, 20(3):213–218, (1997).